

Level Spacing for Resonances of Open Quantum Maps

Rich Wang

Under the direction of
Zhenhao Li
Massachusetts Institute of Technology

Research Science Institute
August 2, 2022

Abstract

Open quantum maps provide a simple finite-dimensional model for open quantum systems. The quantum open baker's map is an example of one such map, and examining the behavior of its eigenvalues gives us an idea about how the frequency and decay of waves in open quantum systems behave. We are especially interested in bounds of the magnitudes of the eigenvalues and their distribution in the complex plane. Bounds on the magnitude for the eigenvalue tell us roughly how quickly waves decay. In this paper, we extend a previous result on spectral gaps to a wider family of maps. We also numerically explore the level spacing distributions of systems with the maximal spectral gap.

Summary

Waves in special environments have two main properties: frequency and decay. By studying a special function that provides us a model for the behavior of these waves, we are able to gain an idea about the behavior of the frequency and decay of waves.

1 Introduction

Open quantum maps effectively model finite-dimensional open quantum chaos. They quantize canonical relations on compact symplectic manifolds allows them to be used effectively for numerical experimentation. The canonical relation we consider is the baker's map, a classical chaotic relation on the unit square. We analyze the quantized version of this relation, which we call the quantum open baker's map. Dyatlov and Jin [1] proved some results regarding the existence of spectral gaps of the quantum open baker's map, but with a singular alphabet. We generalize their results to two alphabets (Theorem 1). We also show the results of our numerical experiments concerning the level spacing distribution of eigenvalues of the quantum open bakers map.

Formally, we define the quantum open baker's map B_N to be an operator on ℓ_N^2 , which is defined by the tuple $(M, \mathcal{A}, \mathcal{B}, \iota, \chi)$, with

$$M \in \mathbb{N}, \quad \mathcal{A}, \mathcal{B} \subset \{0, \dots, M-1\}, \quad \iota: \mathcal{A} \rightarrow \mathcal{B} \quad \chi \in C_0^\infty((0, 1); [0, 1]) \quad (1.1)$$

such that $|\mathcal{A}| = |\mathcal{B}|$ and ι is a bijective function mapping every element in \mathcal{A} to an element in \mathcal{B} . We call M the *base*, \mathcal{A} the *row-alphabet*, \mathcal{B} the *column-alphabet*, ι the *mapping*, and χ the *cutoff function*.

Now let $N = M^k$ for some $k \in \mathbb{N}$. The quantum open baker's map can then be defined as

$$B_N = \mathcal{F}_N^* \begin{pmatrix} \chi_{N/M} \mathcal{F}_{N/M} \chi_{N/M} & & & \\ & \ddots & & \\ & & \chi_{N/M} \mathcal{F}_{N/M} \chi_{N/M} & \\ & & & \chi_{N/M} \mathcal{F}_{N/M} \chi_{N/M} \end{pmatrix} I_{\mathcal{A}, \mathcal{B}, N, M} = \mathcal{F}_N^* J_{\mathcal{A}, \mathcal{B}, N, M}, \quad (1.2)$$

where \mathcal{F}_N is the unitary discrete Fourier transform of size N , $J_{\mathcal{A}, \mathcal{B}, N, M}$ is an N by N matrix, and $I_{\mathcal{A}, \mathcal{B}, N, M}$ is an N by N matrix whose entry in the j -th row and k -th column equals 1 if $\left(\left\lfloor \frac{j}{N/M} \right\rfloor, \left\lfloor \frac{k}{N/M} \right\rfloor\right) \in \iota$, and 0 otherwise.

For example, for the quadruple $(4, \{0, 3\}, \{1, 3\}, \{(0, 1), (3, 3)\}, \chi)$ and $k = 2$,

$$B_N = \mathcal{F}_{16}^* \begin{pmatrix} 0 & \chi_4 \mathcal{F}_4 \chi_4 & 0 & 0 \\ 0 & 0 & 0 & 0 \\ 0 & 0 & 0 & 0 \\ 0 & 0 & 0 & \chi_4 \mathcal{F}_4 \chi_4 \end{pmatrix}.$$

The operator B_N is a discrete analog of a Fourier integral operator of the classical

baker's map, which can be defined on the torus $\mathbb{T}_{x,\xi}^2$ as

$$\varkappa_{M,\mathcal{A}} : (y, \eta) \mapsto (x, \xi) = \left(My - a, \frac{\eta + a}{M} \right),$$

$$(y, \eta) \in \left(\frac{a}{M}, \frac{a+1}{M} \right) \times (0, 1), \quad a \in \mathcal{A}.$$

Papers by Espoti–Nonnenmacher–Winn [2] and Nonnenmacher–Zworski [3] provide a more rigorous study of the analogy between $\varkappa_{M,\mathcal{A}}$ and B_N . For heuristics, one can look to papers by Balázs–Voros [4] and Saraceno–Voros [5].

Because of this analogy, when we perform the quantum open baker's map on such a function f , we expect it to mimic the behavior of a Cantor set. We can define

$$\mathcal{C}_{k,\mathcal{A}} = \mathcal{C}_{k,\mathcal{A}}(M, \mathcal{A}) = \left\{ \sum_{j=0}^{k-1} a_j M^j \mid a_0, a_1, \dots, a_{k-1} \in \mathcal{A} \right\} \in \mathbb{Z}_N, \quad (1.3)$$

$$\mathcal{C}_{k,\mathcal{B}} = \mathcal{C}_{k,\mathcal{B}}(M, \mathcal{B}) = \left\{ \sum_{j=0}^{k-1} b_j M^j \mid b_0, b_1, \dots, b_{k-1} \in \mathcal{B} \right\} \in \mathbb{Z}_N. \quad (1.4)$$

When B_N is applied to typical functions $f \in \ell_N^2$, forward propagation of B_N will produce a graph resembling $\mathcal{C}_{k,\mathcal{A}}$, representing localization in frequency space. Backward propagation of B_N will produce a graph resembling $\mathcal{C}_{k,\mathcal{B}}$, representing localization in position space. An example of this is shown in Figure 1.

Because f can be an eigenvector of B_N , this tells us that all eigenvectors of B_N must already be localized in frequency space to $\mathcal{C}_{k,\mathcal{A}}$.

These eigenvectors and their corresponding eigenvalues are interesting because there exists a correspondence between quantum maps and scattering resonances of waves in certain chaotic systems. The operator B_N is a toy model for the time $t = \log M$ propagator of a quantum system with classical expansion rate 1 [1]. If w is a scattering resonance of the open quantum system with $\text{Im } w \leq 0$ and λ is an eigenvalue of B_N we have that

$$\lambda = e^{-itw} = M^{-i\omega} \rightarrow |\lambda| = M^{\text{Im } \omega} \leq 1.$$

In this paper, we analyze the eigenvalues of B_N , Dyatlov and Jin [1] proved that there exists a spectral gap of B_N when $\mathcal{A} = \mathcal{B}$, and ι is the identity mapping. In

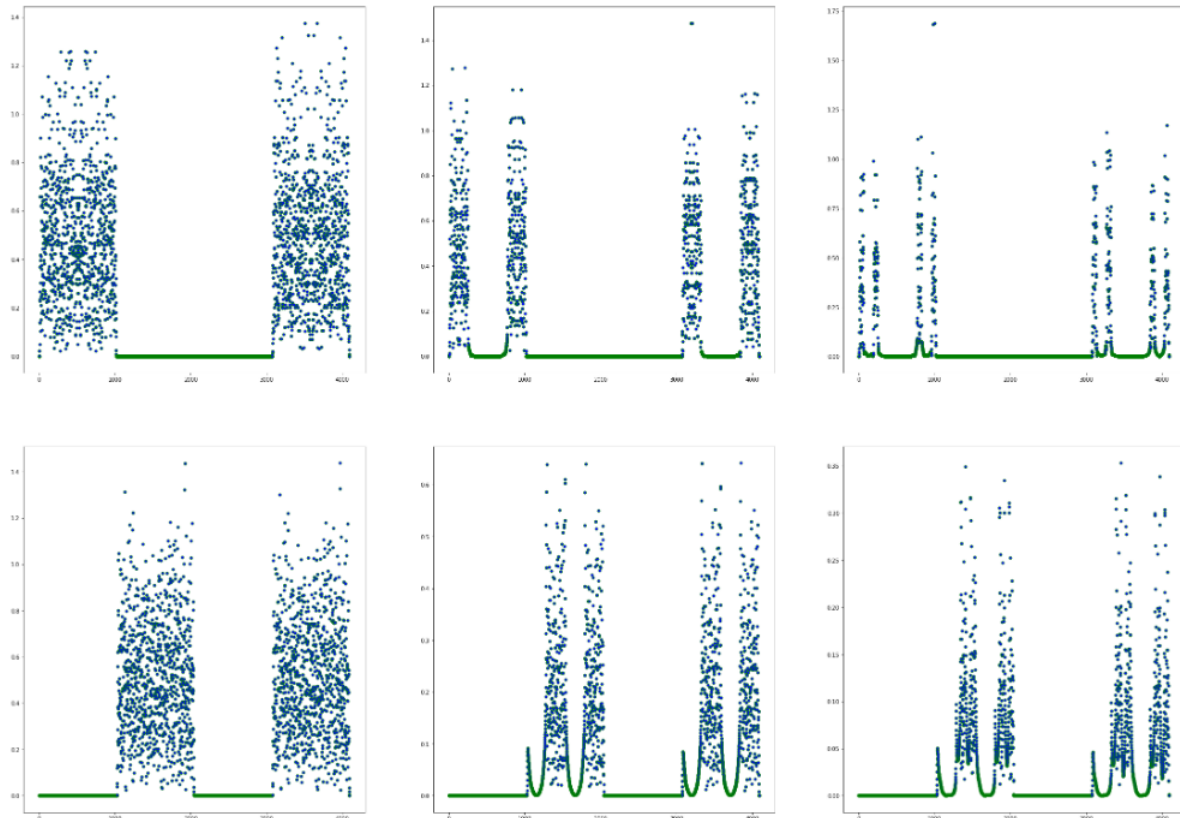


Figure 1: An example of the behavior of B_N and B_N^* , for $M = 4$, $k = 6$, $\mathcal{A} = \{0, 3\}$, $\mathcal{B} = \{1, 3\}$. The j -th diagram in the top row shows what $F_N B_N f$ looks like for a random function f , and j -th diagram in the bottom row shows what $B_N^* f$ looks like for a random function f . The top row shows forward propagation, with f becoming localized in frequency space toward the 1st and 4th Cantor fourths. The bottom row shows backwards propagation, with f becoming localized in position space towards the 2nd and 4th Cantor fourths.

Section 2, we extend this result to general \mathcal{A} and \mathcal{B} . Let

$$r_k = \|\mathbb{1}_{C_{k,\mathcal{A}}} \mathcal{F}_N \mathbb{1}_{C_{k,\mathcal{B}}}\| \quad (1.5)$$

The theorem can then be formally stated below.

Theorem 1. *Define β to be*

$$\beta := - \limsup_{k \rightarrow \infty} \frac{\log(r_k)}{k \log(M)}.$$

If λ is an eigenvalue of B_N , then

$$\lim_{N \rightarrow \infty} \sup \max \{|\lambda| : \lambda \in \text{Sp}(B_N)\} \leq M^{-\beta}. \quad (1.6)$$

Dyatlov and Jin proved a nontrivial spectral gap by using the fractal uncertainty principle [1]. In particular, they showed that

$$\beta > \max \left(0, \frac{1}{2} - \frac{\log |A|}{\log M} \right).$$

In Section 3, we describe our observations on the level spacing distribution of the eigenvalues of B_N , which we observe to be similar to the level spacing distribution of eigenvalues of circular unitary ensembles and circular orthogonal ensembles. We provide some commentary on how we conducted our numerical experiments in Section 4. In Section 5, we discuss the practical applications of the research conducted in our paper.

2 Open Quantum Maps

We generalize the results concerning the spectral radius from Dyatlov and Jin [1] to using 2 alphabets. Many of our definitions are similar, but we include them for completeness.

2.1 Definitions

For $N \in \mathbb{N}$, we define the abelian group $\mathbb{Z}_N := \mathbb{Z}/N\mathbb{Z} = \{0, 1, \dots, N-1\}$, and have the associated ℓ_N^2 space of functions $u : \mathbb{Z}_N \rightarrow \mathbb{C}$, with the norm

$$\|u\|_{\ell_N^2}^2 = \sum_{j=0}^{N-1} |u(j)|^2.$$

The unitary Fourier transform $\mathcal{F}_N : \ell_N^2 \rightarrow \ell_N^2$ is defined as

$$\mathcal{F}_N u(j) = \frac{1}{\sqrt{N}} \sum_{\ell=0}^{N-1} \exp\left(-\frac{2\pi i j \ell}{N}\right) u(\ell).$$

For a cutoff function $\chi : [0, 1] \rightarrow \mathbb{C}$, we define its discretization $\chi_N \in \ell_N^2$ to be

$$\chi_N(j) = \chi\left(\frac{j}{N}\right), \quad j \in \{0, 1, \dots, N-1\}.$$

We fix $(M, \mathcal{A}, \mathcal{B}, \iota, \chi)$ as in 1.1, and define the open quantum map B_N as follows,

$$B_N u(j) = \sum_{(a,b) \in \iota} \sum_{m, \ell=0}^{\frac{N}{M}-1} A_{j\ell}^{ab} u\left(\ell + a \frac{N}{M}\right), \quad (2.1)$$

$$A_{j\ell}^{ab} = \frac{\sqrt{M}}{N} \exp\left(\frac{2\pi i b j}{M}\right) \chi\left(\frac{\ell M}{N}\right) \exp\left(\frac{2\pi i m(j - \ell M)}{N}\right) \chi\left(\frac{mM}{N}\right).$$

We also define the expanding maps Φ_A and Φ_B across the alphabets \mathcal{A} and \mathcal{B} , respectively. More formally,

$$\Phi_A = \Phi_{M, \mathcal{A}} : \bigsqcup_{a \in \mathcal{A}} \left(\frac{a}{M}, \frac{a+1}{M}\right) \rightarrow (0, 1),$$

$$\Phi_B = \Phi_{M, \mathcal{B}} : \bigsqcup_{b \in \mathcal{B}} \left(\frac{b}{M}, \frac{b+1}{M}\right) \rightarrow (0, 1),$$

such that

$$\begin{aligned} \Phi_A(x) &= Mx - a, & x \in \left(\frac{a}{M}, \frac{a+1}{M}\right) \\ \Phi_B(x) &= Mx - b, & x \in \left(\frac{b}{M}, \frac{b+1}{M}\right). \end{aligned} \quad (2.2)$$

The expanding map Φ_A can be thought of as dividing a unit square into N 1 by $\frac{1}{N}$ rectangles, labeling them from 0 to $N-1$, discarding the j -th rectangle for all $j \notin \mathcal{A}$, stretching each remaining rectangle into its own unit square, and stacking each of these unit squares on top of each other. The expanding map Φ_B can be thought of in a similar fashion, but we instead discard the j -th rectangle for all $j \notin \mathcal{B}$.

We denote d to be the distance function on $[0, 1]$, where 0 and 1 are identified with each other. For $x, y \in [0, 1]$,

$$d(x, y) = \min_{k=-1, 0, 1} |x - y - k| = \min\{|x - y|, 1 - |x - y|\}.$$

We also define the distance function over sets, in which it represents the smallest

distance between two elements in those sets. For $x \in [0, 1]$ and sets $U, V \subset [0, 1]$,

$$d(x, V) := \inf_{y \in V} d(x, y), \quad d(V, W) := \inf_{y \in V, z \in W} d(y, z).$$

We now introduce two useful lemmas. The first tells us about how Φ_A and Φ_B interact with d . The second is a nonstationary phase estimate that demonstrates the decay that comes from cancellation when integrating a smooth function against a highly oscillatory function. The proof of both lemmas is well-known [1].

Lemma 2.1. *Assume that $x \in [0, 1]$ and that y is in the domain of Φ . Then*

$$\min\{d(\Phi(y), 0), M \cdot d(y, \Phi^{-1}(x)) \leq d(x, \Phi(y))\}.$$

Lemma 2.2. *Assume that $a \in \mathbb{Z}_N$ and $d\left(\frac{a}{N}, 0\right) \geq cN^{-\rho}$ for some constants $c > 0$, $\rho \in [0, 1]$. Then for all $\chi \in C_0^\infty((0, 1))$, we have*

$$\sum_{m=0}^{N-1} \exp\left(\frac{2\pi iam}{N}\right) \chi\left(\frac{m}{N}\right) = \mathcal{O}(N^{-\infty})$$

where the constants in $\mathcal{O}(N^{-\infty})$ only depend on c , ρ , and χ .

2.2 Propagation of Singularities

For each indicator function $\varphi : [0, 1] \rightarrow \mathbb{R}$, we define

$$\varphi_N \in \ell_N^2, \quad \varphi_N(j) = \varphi\left(\frac{j}{N}\right).$$

The function φ_N is a multiplication operator in ℓ_N^2 . Because we are working in the semiclassical limit, or when $N \rightarrow \infty$, it is convenient to have this notation to allow us to discretize cutoffs. We also define the corresponding Fourier operator

$$\varphi_N^{\mathcal{F}} = \mathcal{F}_N^* \varphi_N \mathcal{F}_N.$$

Dyatlov and Jin proved that the propagation of singularity exists in the one alphabet case, or when forward and backward propagation of B_N look the same [1]. We prove that propagation of singularities exists in the two-alphabet case, or when forward and backward propagation of B_N differ.

Lemma 2.3. *Let $\varphi, \psi : [0, 1] \rightarrow [0, 1]$ be functions. If we have that for some $c > 0$ and*

$0 \leq \rho < 1$,

$$d(\Phi_A(\text{supp } \psi \cap \Phi_A^{-1}(\text{supp } \chi)), \text{supp } \varphi) \geq cN^{-\rho}, \quad (2.3)$$

then,

$$\|\varphi_N B_N \psi_N\|_{\ell_N^2 \rightarrow \ell_N^2} = \mathcal{O}(N^{-\infty}). \quad (2.4)$$

Now say that for some $c > 0$, and $0 \leq \rho < 1$,

$$d(\Phi_B(\text{supp } \psi \cap \Phi_B^{-1}(\text{supp } \chi)), \text{supp } \varphi) \geq cN^{-\rho}. \quad (2.5)$$

Then

$$\|\psi_N^{\mathcal{F}} B_N \varphi_N^{\mathcal{F}}\|_{\ell_N^2 \rightarrow \ell_N^2} = \mathcal{O}(N^{-\infty}), \quad (2.6)$$

where the constants in $\mathcal{O}(N^{-\infty})$ depend only on c , ρ , and χ .

Proof. We first prove 2.4. By 2.1, we know that for all $u \in \ell_N^2$, $j \in \{0, 1, \dots, N-1\}$

$$\begin{aligned} \varphi_N B_N \psi_N u(j) &= \sum_{(a,b) \in \iota} \sum_{\ell=0}^{\frac{N}{M}-1} A_{j\ell}^{ab} u\left(\ell + a\frac{N}{M}\right) \\ A_{j\ell}^{ab} &= \frac{\sqrt{M}}{N} \varphi\left(\frac{j}{N}\right) \exp\left(\frac{2\pi i b j}{M}\right) \chi\left(\frac{\ell M}{N}\right) \psi\left(\frac{\ell}{N} + \frac{a}{M}\right) \tilde{A}_{j\ell}, \\ \tilde{A}_{j\ell} &= \sum_{m=0}^{N/M-1} \exp\left(\frac{2\pi i m(j - \ell M)}{N}\right) \chi\left(\frac{mM}{N}\right). \end{aligned}$$

Defining $r = j - \ell M$ and $\chi_1(x) = \chi(Mx)$, and because $\chi(x) = 0$ for $x \geq 1$, we can write

$$\tilde{A}_{j\ell} = \sum_{m=0}^{N-1} \exp\left(\frac{2\pi i m r}{N}\right) \chi_1\left(\frac{m}{N}\right).$$

Now, $A_{j\ell}^{ab} = 0$ unless $\frac{j}{N} \in \text{supp } \varphi$, $\frac{\ell}{N} + \frac{a}{M} \in \text{supp } \psi$, and $\frac{\ell M}{N} = \Phi_A\left(\frac{\ell}{N} + \frac{a}{M}\right) \in \chi$. Roughly speaking, this restriction on j and ℓ trims away the large elements in B_N , so that we can show that the other entries decay. Along with 2.3, this tells us that

$$d\left(\frac{r}{N}, 0\right) = d\left(\frac{\ell M}{N}, \frac{j}{N}\right) \geq cN^{-\rho}.$$

So now, by Lemma 2.2, we have

$$\|\tilde{A}_{j\ell}\| = \mathcal{O}(N^{-\infty}) \rightarrow \|A_{j\ell}^{ab}\| = \mathcal{O}(N^{-\infty})$$

from which we can see that $\|\varphi_N B_N \psi_N\|_{\ell_N^2 \rightarrow \ell_N^2} = \mathcal{O}(N^{-\infty})$.

We now prove 2.5. In 1.2, we defined $B_N = F_N^* J_{\mathcal{A}, \mathcal{B}, M, N}$. Let $\tilde{B}_N = F_N^* J_{\mathcal{B}, \mathcal{A}, N, M}$. We can show $\|\varphi_N \tilde{B}_N \psi_N\| = \mathcal{O}(N^{-\infty})$ by using \tilde{B}_N in place of B_N and the expanding map Φ_B in place of Φ_A in our proof above. From here, we have that

$$\begin{aligned} \|\psi_N^{\mathcal{F}} B_N \varphi_N^{\mathcal{F}}\|_{\ell_N^2 \rightarrow \ell_N^2} &= \|F_N^* (\psi_N F_N F_N^* J_{\mathcal{A}, \mathcal{B}, N, M} F_N^* \varphi_N) F_N\|_{\ell_N^2 \rightarrow \ell_N^2} \\ &= \left\| F_N^* \left(\overline{\varphi_N F_N^* J_{\mathcal{A}, \mathcal{B}, N, M}^T \psi_N} \right)^* F_N \right\|_{\ell_N^2 \rightarrow \ell_N^2} \\ &= \left\| F_N^* \left(\overline{\varphi_N \tilde{B}_N \psi_N} \right)^* F_N \right\|_{\ell_N^2 \rightarrow \ell_N^2} . \\ &= \mathcal{O}(N^{-\infty}), \end{aligned}$$

which completes the proof. \square

We now generalize Lemma 2.3 to repeated applications of the quantum open baker's map.

Lemma 2.4. *Let $\varphi, \psi : [0, 1] \rightarrow [0, 1]$ be indicator functions. Say that for some $c > 0$, and $0 \leq \rho < 1$, and integer $1 \leq \tilde{k} \leq k$,*

$$d(\text{supp } \psi, \Phi_A^{-\tilde{k}}(\text{supp } \varphi)) \geq cN^{-\rho}. \quad (2.7)$$

Then,

$$\|\varphi_N (B_N)^{\tilde{k}} \psi_N\|_{\ell_N^2 \rightarrow \ell_N^2} = \mathcal{O}(N^{-\infty}). \quad (2.8)$$

And if for some possibly different $0 \leq \rho < 1$, $c > 0$, and integer $1 \leq \tilde{k} \leq k$, we have that

$$d(\text{supp } \psi, \Phi_B^{-\tilde{k}}(\text{supp } \varphi)) \geq cN^{-\rho}. \quad (2.9)$$

Then

$$\|\psi_N^{\mathcal{F}} (B_N)^{\tilde{k}} \varphi_N^{\mathcal{F}}\|_{\ell_N^2 \rightarrow \ell_N^2} = \mathcal{O}(N^{-\infty}), \quad (2.10)$$

where the constants in $\mathcal{O}(N^{-\infty})$ depend only on c , ρ , and χ .

The proof of Lemma 2.4 is identical to that of the corresponding lemma by Dyatlov and Jin [1].

2.3 Spectral Gap

To leave the gap necessary to apply Lemma 2.2, we fix $\rho \in (0, 1)$ and define

$$\tilde{k} = \lceil \rho k \rceil \leq k.$$

We now define sets that represent the localization of $(B_N)^{\tilde{k}}$ on both the frequency and position side. We let

$$\mathcal{X}_{\rho,A} := \{x \in [0, 1] : d(x, \Phi_A^{-\tilde{k}}([0, 1])) \leq N^{-\rho}\},$$

$$\mathcal{X}_{\rho,B} := \{x \in [0, 1] : d(x, \Phi_B^{-\tilde{k}}([0, 1])) \leq N^{-\rho}\}.$$

We now define sets that discretize $\mathcal{X}_{\rho,A}$ and $\mathcal{X}_{\rho,B}$. Using 1.3 and 1.4, we can also define

$$X_{\rho,A} := \bigcup \{\mathcal{C}_{k,A} + m : m \in \mathbb{Z}, |m| \leq 2N^{1-\rho}\} \subset \mathbb{Z}_N,$$

$$X_{\rho,B} := \bigcup \{\mathcal{C}_{k,B} + m : m \in \mathbb{Z}, |m| \leq 2N^{1-\rho}\} \subset \mathbb{Z}_N,$$

With these definitions in place, we proceed with the proof of Theorem 1.

Proof of Theorem 1. We can see that $\varphi \equiv 1$ and $\psi := 1 - \mathcal{X}_{A,\rho}$ satisfy 2.7, so by 2.8, we have

$$(B_N)^{\tilde{k}} = (B_N)^{\tilde{k}} \mathbb{1}_{X_{\rho,A}} + \mathcal{O}(N^{-\infty})_{\ell_N^2 \rightarrow \ell_N^2}, \quad (2.11)$$

Similarly, $\varphi \equiv 1$ and $\psi := 1 - \mathcal{X}_{B,\rho}$ satisfy 2.9, so by 2.10, we have

$$(B_N)^{\tilde{k}} = \mathcal{F}_N^* \mathbb{1}_{X_{\rho,B}} \mathcal{F}_N (B_N)^{\tilde{k}} + \mathcal{O}(N^{-\infty})_{\ell_N^2 \rightarrow \ell_N^2}. \quad (2.12)$$

where the constants in $\mathcal{O}(N^{-\infty})_{\ell_N^2 \rightarrow \ell_N^2}$ only depend on ρ and χ .

Now consider some eigenvalue λ and ℓ_N^2 normalized eigenvector u of B_N . From 2.12 we have

$$\|u - \mathcal{F}_N^* \mathbb{1}_{X_{\rho,B}} \mathcal{F}_N u\|_{\ell_N^2} = \mathcal{O}(N^{-\infty}) \quad (2.13)$$

Combining 2.11 with 2.13 and using the triangle inequality gives us

$$\begin{aligned} \|(B_N)^{\tilde{k}} \mathbb{1}_{X_{k,A}} u - (B_N)^{\tilde{k}} u\|_{\ell_N^2} &= \|(B_N)^{\tilde{k}} \mathbb{1}_{X_{k,A}} u - \lambda^{\tilde{k}} u\|_{\ell_N^2} = \mathcal{O}(N^{-\infty}) \\ \lambda^{\tilde{k}} \|u\|_{\ell_N^2} &\leq \|(B_N)^{\tilde{k}} \mathbb{1}_{X_{k,A}} u\|_{\ell_N^2} + \mathcal{O}(N^{-\infty}) \\ \|(B_N)^{\tilde{k}} (\mathbb{1}_{X_{k,A}} \mathcal{F}_N^* \mathbb{1}_{X_{\rho,B}}) \mathcal{F}_N u\|_{\ell_N^2} &= |\lambda|^{\tilde{k}} \|u\|_{\ell_N^2} + \mathcal{O}(N^{-\infty}) \end{aligned} \quad (2.14)$$

Recall the definition of r_k from 1.5. Because both $(B_N)^{\tilde{k}}$ and \mathcal{F}_N have norm less

than or equal to 1, we look for a bound on the expression

$$\begin{aligned} \mathbb{1}_{X_{k,\mathcal{A}}}\mathcal{F}_N^*\mathbb{1}_{X_{\rho,B}} &\leq \sum_{|m|,|m'|\leq 2N^{1-\rho}} \left\| \left(\mathbb{1}_{C_{k,\mathcal{A}+m}}\mathcal{F}_N^*\mathbb{1}_{C_{\rho,B+m'}} \right) \right\|_{\ell_N^2} \\ &\leq r_k(2 \cdot 2N^{1-\rho} + 1)^2 \\ &\leq 25r_kN^{2(1-\rho)}. \end{aligned}$$

Along with 2.14, this gives us

$$\begin{aligned} |\lambda|^{\tilde{k}} &\leq \left\| (B_N)^{\tilde{k}} \left(\mathbb{1}_{X_{k,\mathcal{A}}}\mathcal{F}_N^*\mathbb{1}_{X_{\rho,B}} \right) \mathcal{F}_N \right\|_{\ell_N^2} \\ &\leq \left\| \left(\mathbb{1}_{X_{k,\mathcal{A}}}\mathcal{F}_N^*\mathbb{1}_{X_{\rho,B}} \right) \right\|_{\ell_N^2} \\ &\leq 25r_kN^{2(1-\rho)}. \end{aligned}$$

as ρ approaches 1, we get an upper bound on $|\lambda|$ equal to $25^{\frac{1}{k}}r_k^{\frac{1}{k}}$. We know that the sequence $\log(r_k)$ is subadditive [1], so applying Fekete's Lemma, we get that

$$\lim_{k \rightarrow \infty} \frac{\log(r_k)}{k} = \inf_{k \geq 1} \frac{r_k}{k}.$$

Thus, if we take the limit as $N = M^k$ approaches infinity, the upper bound on $|\lambda|$ approaches $\inf_{k \geq 1} \frac{r_k}{k}$, showing 1.6. \square

3 Numerical Experiments

In this section, we present numerical evidence showing that the level spacing distribution of the eigenvalues of B_N resembles that spacing distribution of a random orthogonal matrix. This resemblance gives us an idea about the behavior of the decay of waves in open quantum systems. For this section, unless otherwise stated, we assume that $\mathcal{A} = \mathcal{B}$.

3.1 Numerical Evidence for Two Alphabet Results

We present numerical experiments that show that for various special alphabets, the outer spectral gap we proved in Theorem 1 still holds. See Figure 2.

By our work in Section 2, we can now use quantum open baker's maps with 2 distinct alphabets in our numerical experiments, which greatly expands the scope of experiments that we can conduct.

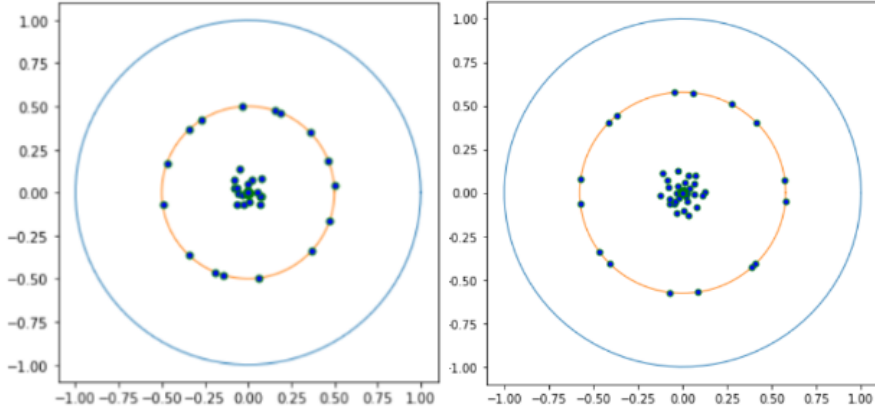


Figure 2: The spectra for $M = 6$, $k = 4$, $\mathcal{A} = \{2, 5\}$, $\mathcal{B} = \{3, 4\}$ is displayed on the left, and the spectra for $M = 8$, $k = 4$, $\mathcal{A} = \{4, 5\}$, $\mathcal{B} = \{2, 6\}$. The eigenvalues in both stay within the first spectral radius, as we proved in Section 2.

3.2 N=KM

In Sections 1 and 2, we have defined $N = M^k$. However, for this section, we redefine $N = KM$, for some $K \in \mathbb{N}$. This does not affect the structure of most of the mathematical objects used in this paper.

We proved in Theorem 1 that when N is an integer power of M , there exists a spectral radius $M^{-\beta}$ of B_N . We claim that a similar result holds when N is an integer multiple of M .

For special alphabets, there is evidence supporting the fact that there exists a spectral radius of $\sqrt{\frac{|\mathcal{A}|}{M}}$. In all of the examples we generated, we identified that this spectral radius holds for when $N = KM$ as well. For example, see Figure 3.

We also noticed that sometimes, the number of eigenvalues along the edge of the first spectral radius tended towards $|\mathcal{A}|^{\lceil \log_M N \rceil}$. This is quite a bit different from our initial prediction of $\lceil |\mathcal{A}|^{\log_M(N)} \rceil$, which would have produced a more direct relationship between the exact value of K and the number of eigenvalues near the first spectral radius.

For some values of K , there is a clear second spectral radius. But for others, there only appears to be one. We have not identified any relationship between which values of N , M , K , \mathcal{A} , and \mathcal{B} produce eigenvalues that create a clear second spectral gap, and which do not, as can be seen in Figure 4.

However, when K is an integer power of M , there always exists a second spectral gap. Numerical evidence suggests that as K approaches an integer power of M , the

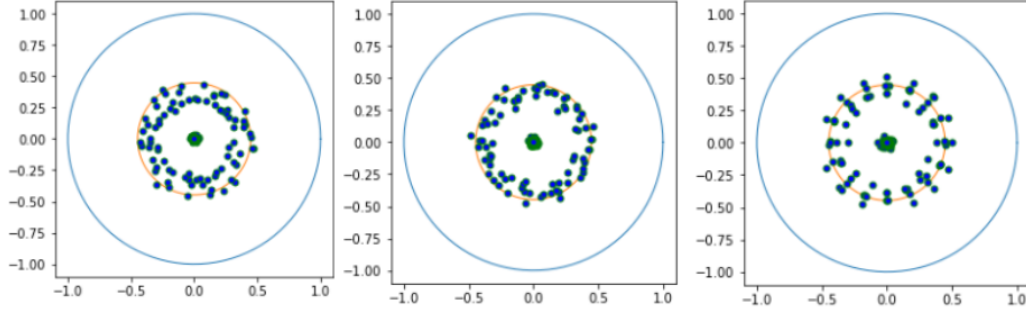


Figure 3: Each plot uses $M = 15$ and $\mathcal{A} = \{2, 7, 12\}$, but from left to right, the values of K used are 420, 480, and 540. Surprisingly, each of these plots has exactly $\lfloor 3^{\lceil \log_1 515K \rceil} \rfloor = 81$ eigenvalues on the first spectral radius, despite having differing values of K .

eigenvalues tend towards the first spectral radius. See Figure 5.

3.3 Level Spacing Distribution

The level spacing distribution of the eigenvalues of B_N has not previously been studied. We suspect that the level spacing distribution of the quantum open baker's map resembles that of a random unitary matrix at times, and a random orthogonal matrix at others. To provide evidence of a possible existing relation, we provide plots of their level spacing distribution and compare the first four moments of each plot. See Figures 6, 7, 8, and 9.

Whether the level spacing distribution of B_N approaches that of a circular unitary ensemble or a circular orthogonal ensemble is likely based off of underlying symmetries that we do not fully understand.

	B_N	CUE		B_N	COE
1st Moment	$1.23 \cdot 10^{-2}$	$1.23 \cdot 10^{-2}$	1st Moment	$9.82 \cdot 10^{-2}$	$9.82 \cdot 10^{-2}$
2nd Moment	$1.81 \cdot 10^{-4}$	$1.78 \cdot 10^{-4}$	2nd Moment	$1.27 \cdot 10^{-2}$	$1.24 \cdot 10^{-2}$
3rd Moment	$3.11 \cdot 10^{-6}$	$2.92 \cdot 10^{-6}$	3rd Moment	$2.03 \cdot 10^{-3}$	$1.84 \cdot 10^{-3}$
4th Moment	$6.06 \cdot 10^{-8}$	$5.29 \cdot 10^{-8}$	4th Moment	$3.87 \cdot 10^{-4}$	$3.12 \cdot 10^{-4}$

The moment tables for Figures 6 and 7.

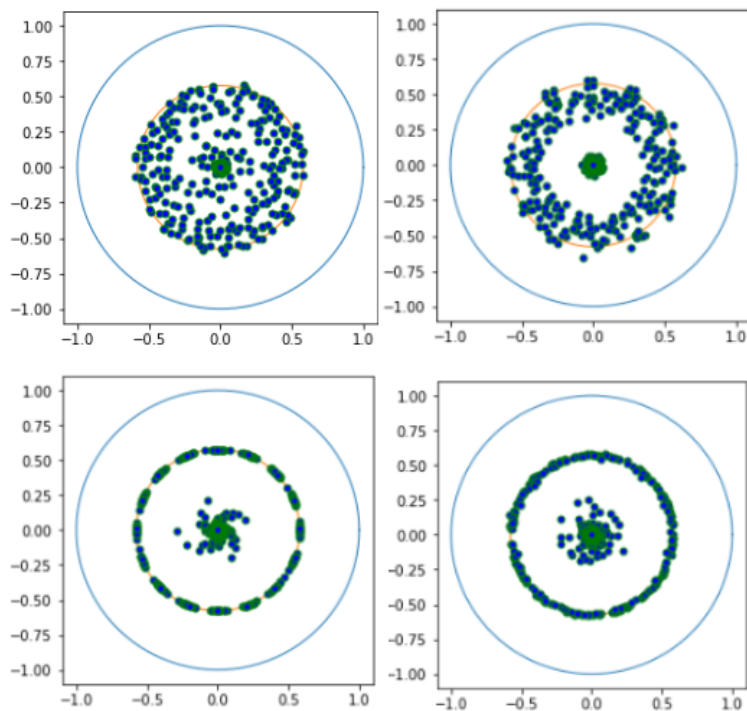


Figure 4: A plot of the eigenvalues for $M = 12$, $\mathcal{A} = \{1, 4, 7, 10\}$, for varying values of K (top left $K = 360$, top right $K = 420$, bottom left $K = 576$, bottom right $K = 588$). It is difficult to tell when exactly there exists a clear second spectral radius.

	B_N	COE		B_N	COE
1st Moment	$9.82 \cdot 10^{-2}$	$9.82 \cdot 10^{-2}$	1st Moment	$9.97 \cdot 10^{-2}$	$9.97 \cdot 10^{-2}$
2nd Moment	$1.47 \cdot 10^{-2}$	$1.24 \cdot 10^{-2}$	2nd Moment	$1.46 \cdot 10^{-2}$	$1.28 \cdot 10^{-2}$
3rd Moment	$2.80 \cdot 10^{-3}$	$1.86 \cdot 10^{-3}$	3rd Moment	$2.74 \cdot 10^{-3}$	$1.94 \cdot 10^{-3}$
4th Moment	$6.05 \cdot 10^{-4}$	$3.18 \cdot 10^{-4}$	4th Moment	$6.09 \cdot 10^{-4}$	$3.34 \cdot 10^{-4}$

The moment tables for Figures 8 and 9.

3.4 Shifting the Alphabet

We observed that when K equals $M^k - M$ for some integer value of K , the eigenvalues of shifted alphabets appears to be equal. We formalize our observation to the following conjecture.

Conjecture 3.1. *Two baker's maps B_N and \tilde{B}_N will have the same spectra if $N = (M^k - M)M$ for some $k \in \mathbb{Z}^+$ and if $\tilde{\mathcal{A}} = \mathcal{A} + m$ for some $m \in \mathbb{Z}$, where \mathcal{A} is the alphabet of B_N and $\tilde{\mathcal{A}}$ is the alphabet of \tilde{B}_N .*

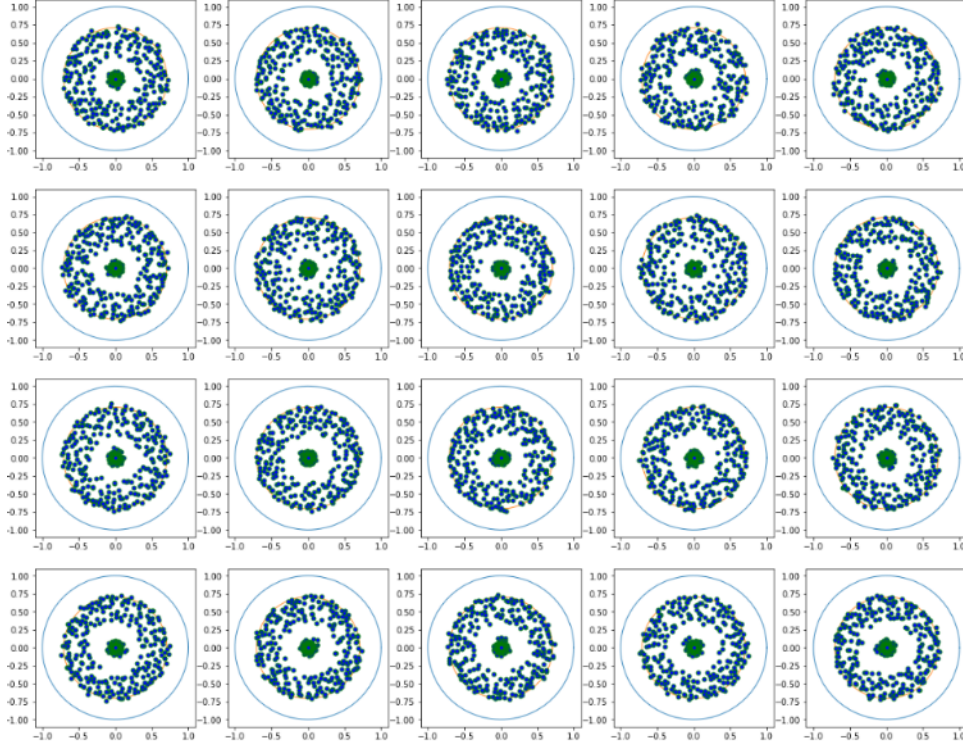


Figure 5: The spectra shown above is for $M = 8$, $\mathcal{A} = \{1, 2, 5, 6\}$, and K ranging from 360 to 379. As K increases, the eigenvalues tend to move closer and closer towards the outer spectral radius.

One can see the the spectra shown in Figures 10 and 11 are identical.

4 Remarks on Numerical Experiments

All numerical experiments were conducted in Python 3, using the numpy package to calculate eigenvalues and the scipy package to generate random circular unitary ensembles and circular orthogonal ensembles. All plots were created using matplotlib.

The cutoff function $\chi_\tau := [0, 1] \rightarrow [0, 1]$ that we used in the numerical experiments conducted in the paper is

$$\chi_\tau(x) = F\left(\frac{x}{\tau}\right) F\left(\frac{1-x}{\tau}\right), \quad F(x) = c \int_{-\infty}^{1.02 \cdot x - 0.01} \mathbb{1}_{[0,1]}(t) e^{-\frac{1}{t(1-t)}} dt,$$

where c is chosen so that $F(x) = 1$ for $x \gg 1$, and τ is chosen such that $\chi_\tau(x) = 1$ for $x \in [\tau, 1 - \tau]$. This cutoff function is effective because it is differentiable, equals 1

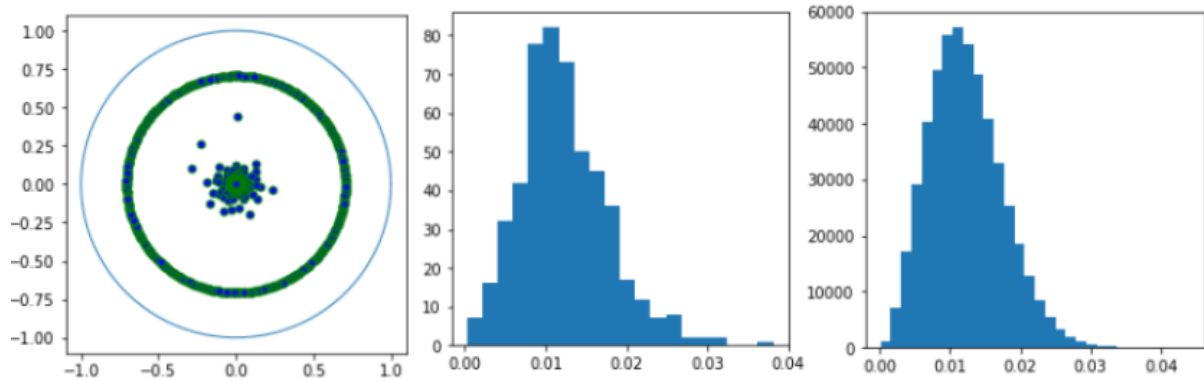


Figure 6: The left two plots are the spectrum and level spacing distribution of eigenvalues for B_N when $M = 16$, $k = 3$, $\mathcal{A} = \{1, 2, 5, 6, 9, 10, 13, 14\}$, and $\mathcal{B} = \{1, 2, 3, 4, 9, 10, 11, 12\}$. The right plot is the level spacing distribution of a 4096 by 4096 circular unitary ensemble.

in the range $[\tau, 1 - \tau]$ for some choice of small τ , and equals 0 everywhere else.

To determine the level spacing distribution of eigenvalues in random circular unitary ensembles of size N , we first generated a thousand random N by N unitary matrices. For each matrix, we computed its eigenvalues, sorted them by their argument, and computed the difference in eigenvalue between each pair of consecutive eigenvalues. We then combined the data from the calculated difference from all hundred matrices, and calculated the moments of this combined data. A similar process was performed for determining the level spacing distribution of eigenvalues in random circular orthogonal ensembles.

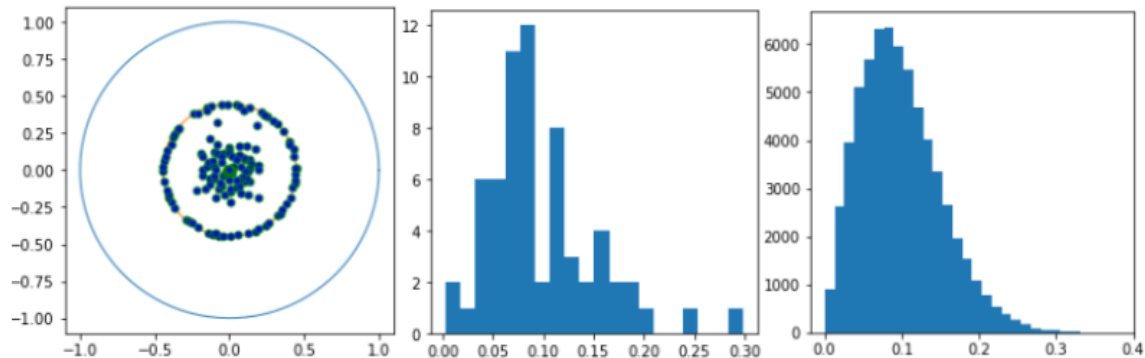


Figure 7: The left two plots are the spectrum and level spacing distribution of eigenvalues for B_N when $M = 20$, $k = 3$, $\mathcal{A} = \{1, 2, 11, 12\}$, and $\mathcal{B} = \{1, 6, 11, 16\}$. The right plot is the level spacing distribution of a 8000 by 8000 circular orthogonal ensemble.

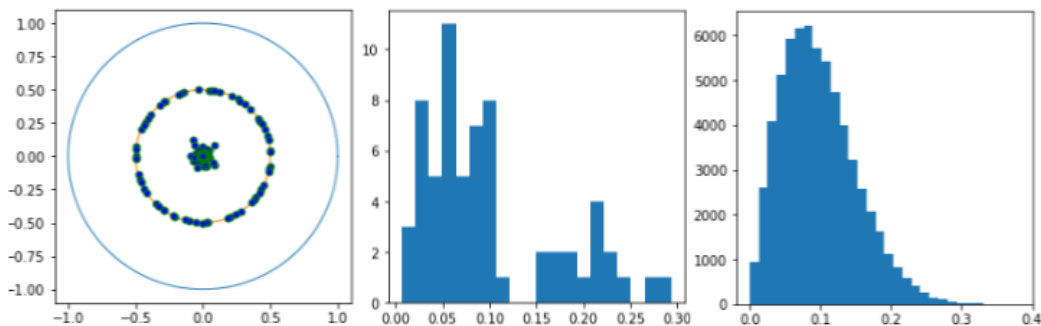


Figure 8: The left two plots are the spectrum and level spacing distribution of eigenvalues for B_N when $M = 16$, $k = 3$, $\mathcal{A} = \{1, 2, 3, 4\}$, and $\mathcal{B} = \{1, 5, 9, 13\}$. The right plot is the level spacing distribution of a 4096 by 4096 circular orthogonal ensemble.

5 Practical Takeaways

The quantum open baker's map is a toy model for Poincaré sections upon which come from scattering Hamiltonians with hyperbolic trapped sets. For details on how specific open quantum systems reduce to open quantum maps, see papers by Nonnenmacher-Sjöstrand-Zworski [6] [7]. Our results on open quantum maps allows us to better understand the behavior the frequency and decay of waves in open quantum systems.

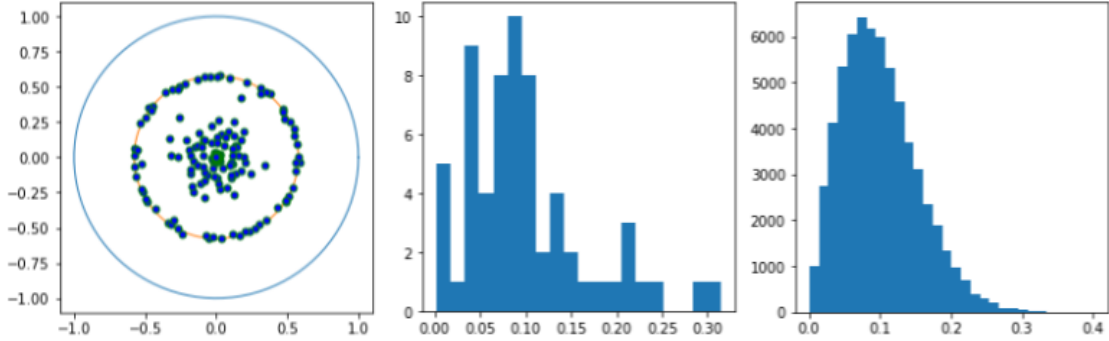


Figure 9: The left two plots are the spectrum and level spacing distribution of eigenvalues for B_N when $M = 12$, $k = 3$, $\mathcal{A} = \{1, 2, 7, 8\}$, and $\mathcal{B} = \{1, 4, 7, 10\}$. The right plot is the level spacing distribution of a 1728 by 1728 circular orthogonal ensemble.

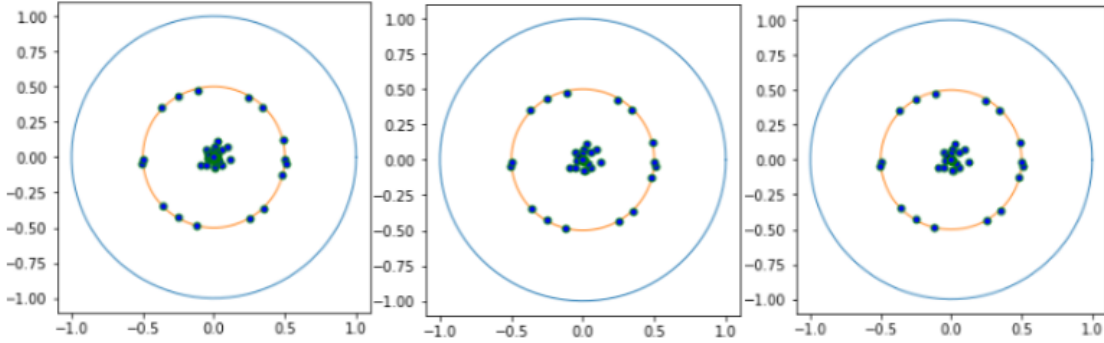


Figure 10: One demonstration of Conjecture 3.1, with $M = 8$ and $K = 8^3 - 8 = 504$, with alphabets $\mathcal{A} = \{1, 3\}$, $\mathcal{A} = \{2, 4\}$, and $\mathcal{A} = \{3, 5\}$, from left to right.

6 Acknowledgments

I would like to thank my mentor Zhenhao Li for suggesting me this project and for guiding me throughout my research. I am also grateful to Dr. Tanya Khovanova and Dr. John Rickert for providing me with paper-writing advice, and the Massachusetts Institute of Technology and the Center of Excellence for Education, for giving me the opportunity to attend the Research Science Institute and conduct this research. Finally, I would like to thank all of my sponsors whose generosity has allowed me to conduct research at the Research Science Institute. Thank you so much to Citadel Securities Campus Sourcing Lead and Campus Recruiting Lead Mr. Fabian Figi, Mr. Alexander Chan, Mr. Alexander Clark, Mr. Steve Meyers, Professor Lauren Meyers, Dr. and Mrs. Philemon D. Chang, Dr. Yongde Luo, and Dr. Weiqin Lu.

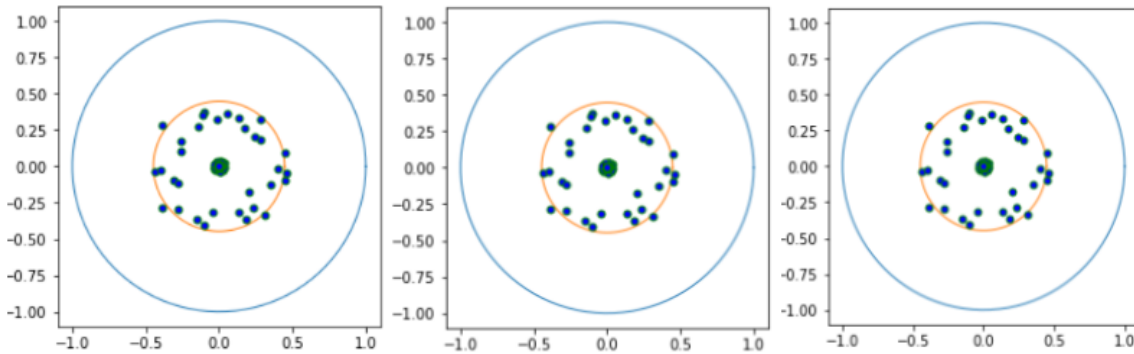


Figure 11: Another example of Conjecture 3.1, with $M = 10$ and $K = 10^3 - 10 = 990$, with alphabets $\mathcal{A} = \{1, 6\}$, $\mathcal{A} = \{2, 7\}$, and $\mathcal{A} = \{3, 8\}$, from left to right.

References

- [1] Dyatlov, S., Jin, L. Resonances for Open Quantum Maps and a Fractal Uncertainty Principle. *Commun. Math. Phys.* 354, 269–316 (2017). <https://doi.org/10.1007/s00220-017-2892-z>
- [2] Mirko Degli Esposti, Stéphane Nonnenmacher, and Brian Winn. Quantum variance and ergodicity for the baker’s map. *Communications in Mathematical Physics*, 263(2):325–352, Feb 2006.
- [3] Stéphane Nonnenmacher and Maciej Zworski. Distribution of resonances for open quantum maps. *Communications in Mathematical Physics*, 269(2):311–365, Nov 2006.
- [4] Nándor L. Balázs and André Voros. The quantized baker’s transformation. *Annals of Physics*, 190(1):1–31, 1989.
- [5] Marcos Saraceno and André Voros. Towards a semiclassical theory of the quantum baker’s map. *Physica D: Nonlinear Phenomena*, 79(2):206–268, 1994.
- [6] Stéphane Nonnenmacher, Johannes Sjöstrand, and Maciej Zworski. From open quantum systems to open quantum maps. *Communications in Mathematical Physics*, 304(1):1–48, Mar 2011.
- [7] Stéphane Nonnenmacher, Johannes Sjöstrand, and Maciej Zworski. Fractal weyl law for open quantum chaotic maps. *Annals of Mathematics*, 179(1):179–251, 2014.